Phase Transitions and Surface Morphology of Surfactant-Coated Aerosol Particles

Ephraim Woods III,* Hannah S. Kim, Carl N. Wivagg, Sarah J. Dotson, Keith E. Broekhuizen, and Erin F. Frohardt

Department of Chemistry, Colgate University, 13 Oak Drive, Hamilton, New York 13346

Received: June 21, 2007; In Final Form: August 9, 2007

Probe molecule spectroscopy and hygroscopic growth curves characterize the morphology of surfactant-coated aerosol particles as a function of relative humidity (RH). This study focuses on particles composed of either potassium iodide or sodium chloride and sodium dodecyl sulfate (SDS). At high RH, these mixed particles assume a reverse micelle type structure, and at low RH, they comprise a solid core of either KI or NaCl coated with SDS and water. The deliquescence relative humidity (DRH) and efflorescence relative humidity (ERH) of the inorganic fraction of the mixed particles are very similar to those of the pure salts. The surface polarity and morphology sampled by the coumarin 314 probe molecule ranges from that of a water−organic interface to that of an ionic surface and depends strongly on the RH and the amount of SDS. When the SDS coverage of the droplet just prior to efflorescence reaches approximately one monolayer, a thin soap film persists on the surface to values of RH much lower than the ERH. Both the electronic spectroscopy and photoelectric charging efficiency show a separate efflorescence for this layer at RH < 5%. The spectroscopy further reveals that there is a hysteresis associated with this low RH phase transition for both KI and NaCl cores.

I. Introduction

Aerosol particles play an important role in the atmosphere, affecting the earth's radiation budget directly through light scattering and indirectly through the nucleation of cloud droplets. Particles also serve as centers for heterogeneous chemical reactions, many of which greatly affect the composition of the atmosphere. Both aspects may be affected by the presence of organic molecules on the particles, and field measurements show that a large fraction of tropospheric particles have an appreciable organic component.[1,2] Marine aerosols, in particular, are found to be coated with amphiphilic molecules such as palmitic acid and other long chain acids.[3,4] Even particles of continental origin, such as sulfate, sometimes carry similar coatings.[5] The consequences for the atmosphere of these internally mixed particles represent an obstacle in producing accurate atmospheric models. As a further complication, the morphology of these particles has been shown to be as important as the composition in determining the reactivity of the particle.

An example of this morphology dependence is the reaction of particle-bound oleic acid, a common product of meat cooking, with ozone. Several groups report the heterogeneous kinetics of this reaction using neat oleic acid particles.[6−9] Each of the experiments measure reaction rates that predict a short lifetime for oleic acid in the atmosphere, contrary to observations.[10] One conclusion of these experiments is that neat oleic acid makes a poor proxy for real atmospheric particles—the morphology of the particles matters.

Another example that is particularly pertinent to this work is the reactive uptake of N_2O_5 onto aqueous droplets coated with either hexanoic acid[11] or sodium dodecyl sulfate (SDS).[12] The reverse micelle type morphology modeled in those experiments serves as a model for marine aerosol particles.[13] This experiment demonstrates that organic coatings can inhibit the rate of uptake of reactive gases by as much as an order of magnitude.[12]

Although there are many variables that influence particle morphology, the relative humidity (RH) is among the most important. It can alter the water content and drive phase changes in particles of soluble salts.[14] The hygroscopic growth of particles with organic components with changing RH is complex. Some neat organic acid particles have been shown to deliquesce and effloresce,[15,16] and their ERH's are as low as 5% RH.[16] Several researchers show that the phase transitions of internally mixed particles are relatively unperturbed by small amounts of organic constituents.[17−20] Though the growth factors are often suppressed by organic coatings, the DRH and ERH of the particles change very little. For example, the DRH of NaCl particles mixed with SDS is only a few percent different than it is for the neat NaCl particles.[20] When the organic fraction is water-soluble, the DRH is slightly smaller than for the neat particles, whereas the ERH may be either greater or smaller. The character of the mixed particles at a RH lower than the ERH is relatively unexplored. Our goal is to characterize the morphology of mixed inorganic−organic aerosols that model reverse micelle aerosols across a wide range of RH.

This paper introduces a novel method of using probe molecule spectroscopy to study the surface morphology and phase behavior of aerosol particles. Previous efforts to investigate phase changes in aerosols with molecular probes used florescence to measure the amount of free and solvated water in the particle.[21,22] We use two complementary measurements to assess the chemical environment of our probe molecule, coumarin 314 (C314), as a means of characterizing the surface of these particles. Using a two-step laser ionization scheme, we measure both the electronic excitation spectrum of the probe and the relative photoelectric charging efficiency of the particle as a function of RH. The electronic excitation spectrum of the probe measures the polarity of the particle surface, and we have

* Corresponding author. E-mail: ewoods@mail.colgate.edu.

10.1021/jp074848m CCC: $37.00
Published on Web 10/11/2007

recently employed this approach to measure the surface polarity of several model aerosol particles.[23] As we will show, the photoelectric charging efficiency of the particle is a reflection of the surface's ability to capture the nascent photoelectron produced by the C314. As such, it is sensitive to changes in the particle's morphology. To provide a reference for these novel methods, we measure the hygroscopic growth curves of our test particles using a relative humidity tandem differential mobility analysis (RH-TDMA) instrument, which is a well-tested tool for investigating phase transitions in aerosol particles.

We have chosen to study soluble salts (KI and NaCl) internally mixed with the surfactant, SDS. Because of the large ionic strength and high surface area to volume ratio of these particles in the aqueous phase, the SDS molecules reside almost exclusively on the surface of the particles. At high RH values, then, these particles assume a reverse micelle type morphology, with the SDS coating an aqueous core of either KI or NaCl. With falling RH, the particles lose water and the concentration of the aqueous core increases, as does the surface density of SDS. At low RH, these particles comprise a solid salt core with SDS and water adsorbed on the surface. Like the SDS, the C314 probe molecule is surface active, so our experiment probes the morphology of these particles near the surface. Clearly, NaCl is an important component of marine aerosol. The other salt, KI, is not abundant in the atmosphere, but it is especially convenient in our study because of its strong interaction with C314.

II. Experimental Section

Aerosol Photoionization. The aerosol photoionization spectra and photoelectric charging efficiency[24−26] curves are recorded using a two-step ionization scheme. Previous publications describe in detail the apparatus used to collect these data.[23,27] Briefly, an atomizer produces an atmospheric pressure flow of aerosol particles from a homogeneous solution of salt (either NaCl or KI), SDS, and trace amounts of C314. A 0.4 slpm portion of this flow enters a diffusion dryer where the RH drops to approximately 10%, followed by a static control ionizer (NRD), which brings the particles into charge equilibrium. A DMA, running with a sheath flow of 4.0 slpm, size selects the dried flow, and typical particles diameters are 70−100 nm.

Following the size-selection stage, the flow system differs between two schemes, "deliquescence mode" and "efflorescence mode". In the former, a flow of dry air first dilutes and further dries the particles to RH < 2%, and a second, approximately 90% RH flow adjusts the final RH to the desired value. In this mode, the fully dried particles never experience a higher RH than the one where the measurement ultimately takes place. In efflorescence mode, the size-selected particles flow through a flask that is partially filled with liquid water. The residence time through the flask is approximately 30 s, and the RH of the particles after passing through the flask is >80%. The exposure to high RH is adequate to deliquesce the particles in the flow. A 4.0 slpm, RH-controlled flow then dilutes the flow and decreases the RH to its ultimate value. In efflorescence mode, the size-selected particles never experience a lower RH than the one targeted for measurement. In both modes, the particles pass through an empty volume, allowing them to experience their ultimate RH for approximately 30 s prior to analysis.

For the photoionization spectroscopy experiment, the particle flow interacts with two co-propagating laser beams in an ionization cell. A tunable visible laser beam excites the S_1 state of C314 and an ultraviolet laser beam ionizes only those molecules that are electronically excited. A Nd:YAG-pumped optical parametric oscillator produces the tunable visible light, and a second, frequency-tripled Nd:YAG produces the 355 nm, ultraviolet light. A small electric field (∼10 V/cm) precipitates the nascent photoelectrons but does not significantly perturb the trajectory of the particles. The resulting positively charged aerosol flow passes through an aerosol electrometer (TSI model 3065A), which measures the charge in the flow. Monitoring the amount of charge in the flow while scanning the visible laser's wavelength produces the aerosol photoionization spectrum. Because only the electronically excited molecules contribute to the two-laser signal, the photoionization spectrum reflects the absorption spectrum of the excited state.

The photoelectric charging efficiency experiment is similar. In this case, we fix the wavelength of the visible laser to match the maximum of the photoionization spectrum and measure the signal intensity as a function of RH. We find that the signal is linear with the particle concentration over the small range of concentrations sampled in our experiment. Thus, for each value of RH, we normalize the signal to the particle concentration, measured by the electrometer current in the absence of lasers.

RH-TDMA. The relative humidity tandem differential mobility analyzer experiment (RH-TDMA) is similar to arrangements reported in detail previously,[28,29] so we provide only a short summary of the approach. An atomizer produces particles from a dilute aqueous solution of either KI or NaCl with sodium dodecyl sulfate (SDS). A diffusion drier filled with silica gel dries the particle flow to approximately 10% RH, and the first DMA size selects a portion of the dried flow for analysis. We typically use "dry sizes" in the range of 75−100 nm with a geometric standard deviation of 1.05−1.1.

The labels, deliquescence mode and efflorescence mode, have the same meaning here as with the photoionization experiment. In an efflorescence mode experiment, the dried flow passes through a flask containing liquid water where the particles deliquesce. The resulting flow then equilibrates with a RH-controlled flow, and the particles reach their ultimate size. A scanning mobility particle sizer (SMPS, Grimm Scientific), equipped with a second DMA and a condensation particle counter, analyzes the final size distribution of the aerosol. In this arrangement, the particles reach their ultimate RH from a higher RH value. In a deliquescence mode experiment, the aerosols bypass the flask and reach their ultimate RH from a lower RH value.

III. Results

Hygroscopic Growth. Our primary interest is the surface morphology of these particles. We first present the hygroscopic growth curves of these particles as a characterization of the bulk phase behavior and as a reference for our spectroscopic methods. Figure 1 shows the results of the RH-TDMA experiment for pure KI, pure NaCl, KI/SDS and NaCl/SDS mixtures, and Table 1 summarizes the data. The mobility growth factors plotted in Figure 1 represent the ratio of the final mean diameter to that of the dry size selected by the first DMA. The source solution composition for the pure salts is 3.0 g/L of NaCl or KI. The NaCl/SDS and KI/SDS mixtures are 3.0 g/L of salt and 0.150 g/L SDS.

The DRH and ERH values for pure NaCl, 76% and 42% respectively, are within experimental error of several other measurements.[14,30−33] For the mixed NaCl/SDS system, which has also been investigated previously,[20] the deliquescence point is nearly unchanged, as would be expected for this small concentration of SDS. The ERH rises slightly, from 42% to 45% RH, relative to the pure NaCl particle. There are no

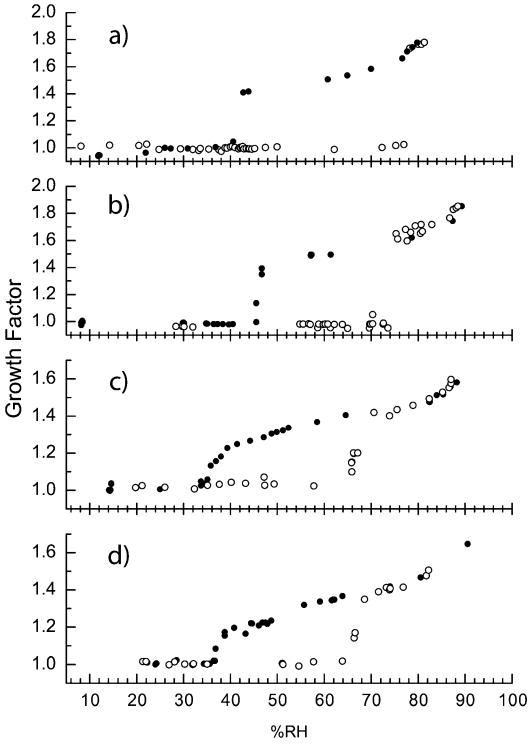

Figure 1. Hygroscopic growth curves for (a) NaCl, (b) NaCl/SDS, (c) KI, and (d) KI/SDS. In each case, the filled circles represent the efflorescence mode and the open circles represent the deliquescence mode. The mobility growth factors represent the ratio of the measured mean particle size to the mean dry size.

TABLE 1: Deliquescence and Efflorescence Relative Humidities of Salt and Salt−SDS Mixtures

sample	DRH	ERH	lit. DRH	lit. ERH
NaCl	76 ± 2	42 ± 2	75−75.7[a]	40−45[a]
NaCl/SDS (4.8%)	75 ± 2	45 ± 2	76[b]	
KI	67 ± 2	38 ± 2		
KI/SDS (4.8%)	66 ± 2	38 ± 2		

[a] Taken from ref 28. [b] Taken from ref 18.

previous measurements for either neat KI or KI/SDS. The DRH for both the pure and mixed particle is near 66% RH. This value is much lower than that of NaCl, a result of its greater solubility (8.3 mol/L for KI vs 4.0 mol/L for NaCl at 298 K). Both the KI and KI/SDS efflorescence curves exhibit a comparatively gradual change from the aqueous to solid state between 36 and 39% RH. Perhaps the loss of water is not as facile kinetically for the KI case as it is for NaCl, and the equilibration time of particles in our experiment (30 s) limits the resolution of the ERH. These experiments establish the bulk phase behavior of these particles and aid in the interpretation of the aerosol photoionization data.

Photoelectric Charging Efficiency—KI/SDS. Figure 2 shows the relative photoelectric charging efficiency (ϕ_{rel}) of KI/SDS aerosol particles as a function of RH in efflorescence mode. These data correspond to a source solution of 3.0 g/L KI and 0.150 g/L SDS, which produces a dry particle that is 4.8% SDS by mass. Bypassing the deliquescence flask produces the additional point at 0%. The hygrometer is not accurate for RH less than 5%, so the 0% label is nominal. Dividing the total signal by the signal in the absence of lasers, which reflects the concentration of singly charged particles in the flow, yields the value of ϕ_{rel}. We normalize the value such that the minimum signal is set to 1.0; therefore, a value of 1.2 on the *y*-axis means

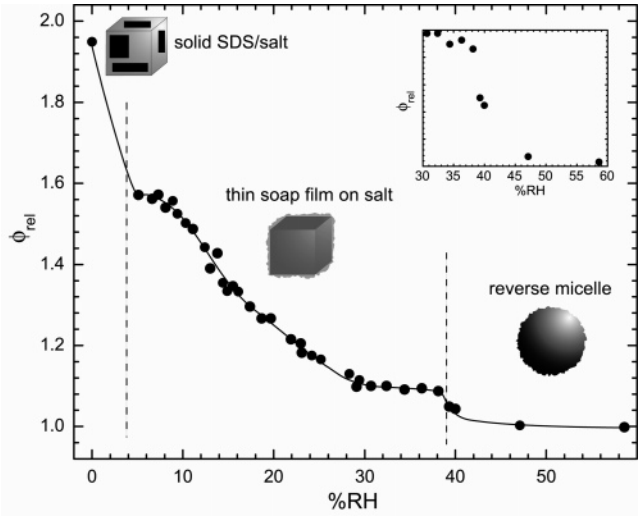

Figure 2. Relative photoelectric charging efficiency (ϕ_{rel}) curves for KI/SDS (4.8%) taken in the efflorescence mode. The solid line is a guide to the eye, and the vertical lines mark the transitions between proposed morphologies: reverse micelle (>40% RH), thin soap film on KI crystal (5−40% RH), and solid KI/SDS (<5% RH). The inset shows the 30−60% RH range with an expanded ϕ_{rel} scale.

that we measured 20% more ionization signal at that RH than for the reference case. The absolute value of ϕ depends on several experimental factors including laser alignment, laser power, and particle size distribution. As such, it is less well-determined than the relative magnitudes within a particular data set. Consistent with efflorescence mode experiments, we consider the changes in the signal from the point of view of falling RH.

The ϕ_{rel} curve increases monotonically with decreasing RH from 60% RH to 0% RH. As discussed in more detail later, we attribute the increase of the signal with falling RH in large part to the desorption of water in the vicinity of the probe molecule. Adsorbed water can capture nascent photoelectrons from the probe molecule, preventing the particle from becoming charged. In addition to the smooth changes associated with the desorption of water, the data show two more abrupt changes. Specifically, there is a sharp change between 38 and 40% RH and also between 0% and 5% RH. These features imply substantial changes in the environment of the probe molecule and reflect morphological changes on the surface that accompany the loss of water.

To better interpret the shape of ϕ_{rel}, we compare this result to that for different KI/SDS mixtures. Figure 3 compares the results for four different particles: pure KI, and three mixtures with compositions of 1.6%, 3.2%, and 4.8% SDS. Again, the mass percent is given relative to the total dry solute mass, because the total mass depends on RH. The 4.8% SDS dataset is the same as in Figure 2. These data are scaled and offset to facilitate comparisons in the shape of the curves.

For pure KI, the top trace in the figure, ϕ_{rel} is nearly flat for RH > 40% but sharply increases when the RH drops below 38% RH. The transition between these domains is within experimental error of the ERH measured using RH-TDMA, and we attribute this feature to efflorescence. As the RH decreases below the ERH, the efficiency grows gradually and monotonically to its maximum value near 0%. Comparing the pure KI case to the 4.8% SDS case, the bottom trace in the figure, reveals two main differences. First, the curvature of data between 38% and 15% RH is more positive for the mixed particle. Second, the aforementioned sharp change in the ionization efficiency

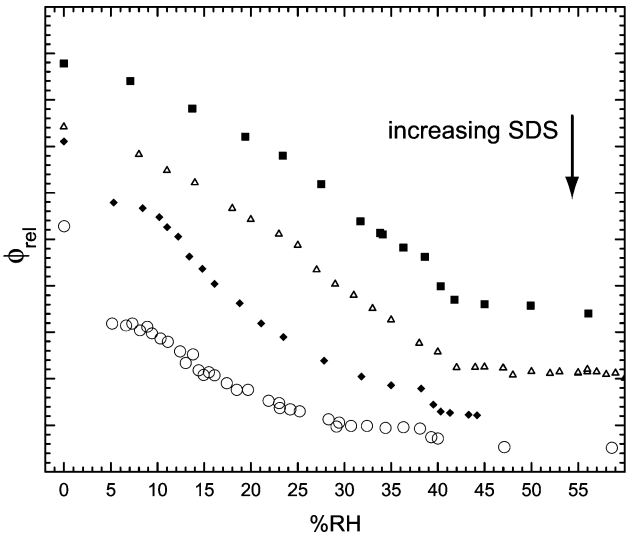

Figure 3. Comparison of ϕ_{rel} for four KI/SDS mixtures. The SDS compositions are 0% (■), 1.6% (Δ), 3.2% (◆), and 4.8% (○) by mass in the dry particle. The data are scaled and offset to facilitate comparison. Low coverages of SDS show no sharp transition near 5% RH, whereas larger coverages do.

between 0 and 5% RH for the mixed particles is absent in the pure KI case.

The 1.6% and 3.2% SDS mixtures demonstrate a transition between the two cases. For the 1.6% mixture, the shape is very similar to pure KI but with a slightly lower ionization efficiency. For the 3.2% mixture, the shape is more similar to the 4.8% data. In general, for these mixtures, the photoelectric charging efficiency decreases with increasing SDS concentration by approximately a factor of 2.5 over the range in concentration in our experiment.

In deliquescence mode, the data are similarly monotonic with changing RH; however, the curves do not exhibit any sharp structure. We conclude that the amount of adsorbed water changes continuously with changing RH, producing no qualitative changes in the morphology of the particle until reaching the deliquescence point. These results further suggest that both of the sharp changes in the efflorescence mode curves arise from efflorescence processes, which would not be observed in the deliquescence mode experiments. Clearly, the feature in the efflorescence mode data at 38% RH corresponds to the crystallization of the KI. The feature at lower RH, then, must correspond with changes in the SDS.

Aerosol Photoionization Spectra—KI/SDS. The electronic spectroscopy of C314 is a probe of the polarity of its surroundings. We track changes in the spectroscopy with changing RH to provide a qualitative description of the particle morphology. Figure 4 shows a series of photoionization spectra of C314 near the surface of KI/SDS particles collected with several values of RH. For RH of 50% and 70%, both above the ERH, we expect the particle assumes the reverse micelle type morphology. The other two values of RH, 20% and 0%, are below the ERH, and reflect solid KI coated in some fashion by SDS and/or water. All of the spectra represent efflorescence mode data collection with the exception of the 20% frame, which includes a spectrum collected in deliquescence mode. For each spectrum, we fit the data with an arbitrary function that represents the spectrum well and assign the maximum of the fitted curve as the wavelength of maximum absorption, λ_{max}.

The frame displaying the 70% spectrum also marks the λ_{max} for C314 dissolved in water (449 nm) and benzene (430 nm). These two homogeneous solvents represent nonpolar and polar references for these interfacial systems. The λ_{max} value near 440 nm for both the 70% and 50% spectra is an intermediate value, which is consistent with the likely position of the probe molecule at the water−organic interface of the reverse micelle particle. The polarity of interfacial regions are often found to be intermediate between the two bulk phases,[34] as it is in this case. In some cases, strongly interacting liquid−liquid interfaces can produce regions whose polarity varies in a non-additive way from the bulk phases. For example, the water−1-octanol interface is characterized by an alkane-like region that is less polar than either bulk water or 1-octanol.[35] A similar alkane-like region likely exists at the surface of these coated particles, as well. We can infer from our experiments that the C314 probe molecules do not sample this environment but reside near the sulfate head groups and interact with water.

In efflorescence mode at 20% RH, the λ_{max} value is similar to the 50% and 70% RH value, indicating that the chemical environment of the probe molecule is similar in each case. This result is a strong indication that there is sufficient water remaining on the particle after the crystallization of the KI to produce a similar water−organic interface to the reverse micelle type morphology observed for RH > ERH. We propose that, following efflorescence of the KI, the particle comprises a solid KI core in equilibrium with a thin film of water and SDS. Here, the deliquescence mode spectrum is distinctly red-shifted from the efflorescence mode spectrum. This spectrum resembles more closely that for C314 adsorbed to pure KI ($\lambda_{max} \sim 450$ nm). The observation that the photoionization spectrum at 20% RH depends on the history of the particle is conclusive evidence that there is a phase transition at some lower RH. It is analogous to the observation of two distinct particle morphologies (aqueous or crystalline) for RH between that of the ERH and DRH for single component particles. The bottom panel shows the results for a RH = 0%. This RH is beyond the low RH phase transition, and in this case, the spectrum also resembles the C314 spectrum for pure KI.

Figure 5 illustrates the hysteresis that arises from this low RH phase transition as reflected by the excited-state spectroscopy. The figure plots the λ_{max} value as a function of RH in both efflorescence and deliquescence mode. In efflorescence mode, the λ_{max} is consistently near 440 nm until the low RH phase transition where it jumps to 446 nm, similar to the pure KI value. In deliquescence mode, the λ_{max} value decreases slowly with increasing RH but does not match the efflorescence curve. We observe only a small decrease in λ_{max} over this range, consistent with the adsorption of water but not the formation of a uniform water−organic interface as found in the efflorescence mode. At the 60% RH, which is close to the DRH, the λ_{max} returns to the lower value associated with the water−organic interface. Although this hysteresis loop, in general, should depend on the age of the particles, our results are constant over the short range of timescales we can sample (~1 min).

Though the C314 spectroscopy is not particularly sensitive to the crystallization of the KI, it is sensitive to the changes in the SDS fraction on the surface of the KI solid. Conversely, the hygroscopic growth curves reveal the deliquescence and efflorescence of the KI component, but the size changes associated with the SDS fraction are too small to be observed. The ionization efficiency data reveal both phase transitions.

Threshold for Thin Film Formation. Figure 3 suggests that 1.6% SDS is an insufficient amount to produce the thin SDS film that we propose explains the hysteresis at low RH. The shape of the curve is similar to that for pure KI, and there is no evidence of a phase transition at low RH. Intuitively, we expect

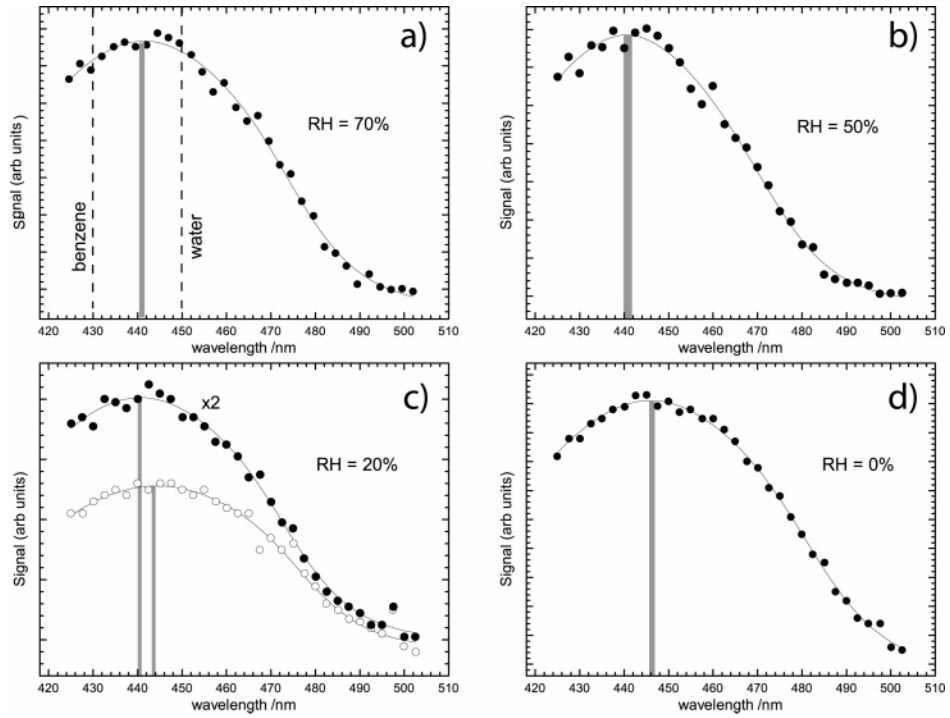

Figure 4. Photoionization spectra for KI/SDS (4.8%) for (a) 70% RH, (b) 50%, (c) 20%, and (d) 0%. The position of the vertical lines mark the fitted value of λ_{max}, and the width represents the standard error in the fit. For (a), vertical lines also mark λ_{max} values for C314 dissolved in benzene and water for comparison. Panel c shows both efflorescence mode (●) and deliquescence mode (○) data.

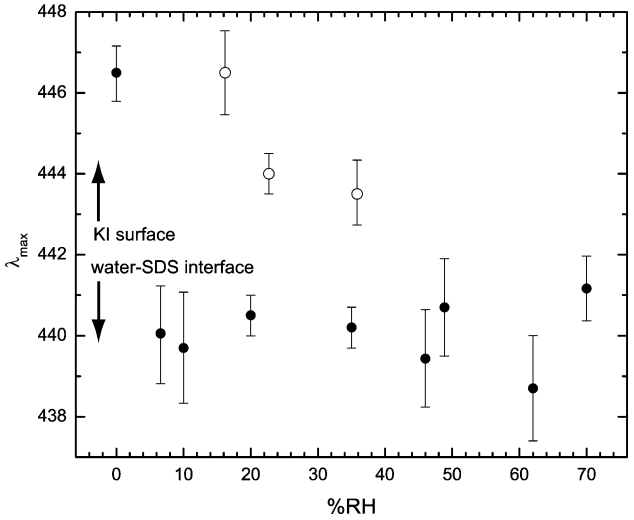

Figure 5. λ_{max} values for KI/SDS (4.8%) as a function of RH in efflorescence mode (●) and deliquescence mode (○). These data demonstrate that the surface morphology sampled by the probe molecule depends on the history of the particle over a large range of RH.

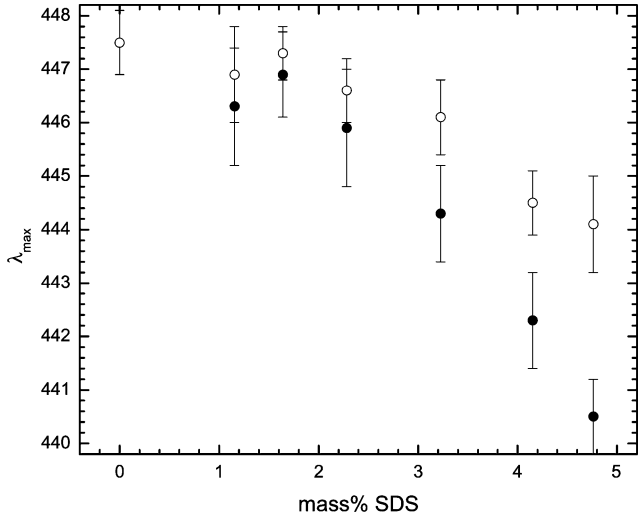

Figure 6. λ_{max} values for KI/SDS mixtures as a function of mass % SDS in efflorescence mode (●) and deliquescence mode (○). Small coverages of SDS do not produce the hysteresis behavior, but large coverages do. The threshold value for observing the hysteresis is 2−3% SDS.

that particles with only trace amounts of SDS should behave very similarly to pure KI. As a measure of the threshold amount of SDS necessary to produce the thin film, we record the excited-state spectroscopy in both efflorescence and deliquescence modes at 20% RH for several SDS concentrations. When the thin film forms, as Figure 5 shows, these values are different; whereas, for pure KI, they are the same. Figure 6 shows the λ_{max} values at 20% RH vs SDS concentration recorded in both efflorescence and deliquescence mode. The data indicate that the hysteresis effect appears in the range of 2−3% by mass SDS.

NaCl Results. Figures 7 and 8 show efflorescence mode ϕ_{rel} curves and λ_{max} data for NaCl/SDS mixtures, respectively. The ionization efficiency curve in Figure 7 also shows the data for pure NaCl for comparison. As with KI, there is an increase in ϕ_{rel} at the normal ERH (∼45%) for both pure NaCl and with a mixture that is 4.8% SDS. In fact, the two curves are nearly superimposable for RH between 30% and 60%. Below 30%, ϕ_{rel} is fairly flat for pure NaCl but is more sloped for the mixture. Smaller signals with the NaCl-containing particles limit our ability to dilute the aerosol flow and, thus, the range of RH investigated for these systems. As a result, we cannot find direct evidence of a low RH phase transition associated with SDS layer from the ϕ_{rel} data. The λ_{max} data reveal that there is a similar effect, though. Figure 8 shows that the λ_{max} value at 20% RH depends on the mode of collection, indicating that a phase transition must occur at some lower RH. The difference in λ_{max} is smaller than for KI, but that is an expected result. The NaCl

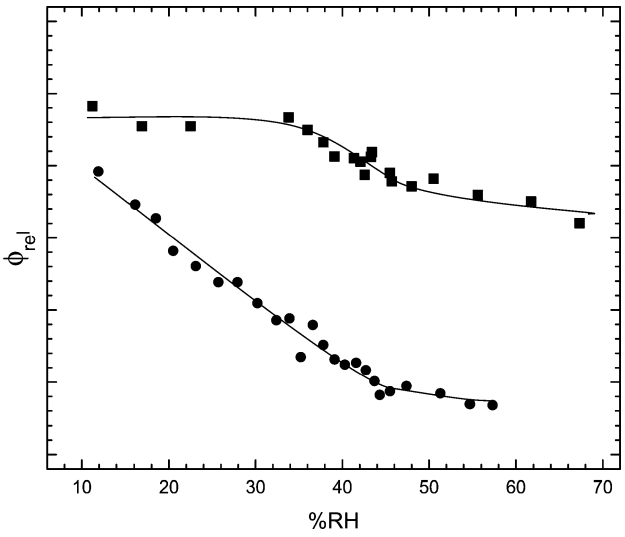

Figure 7. Comparison of ϕ_{rel} for neat NaCl and NaCl/SDS (4.8%). The data are scaled and offset to facilitate comparison, and the solid lines are a guide to the eye.

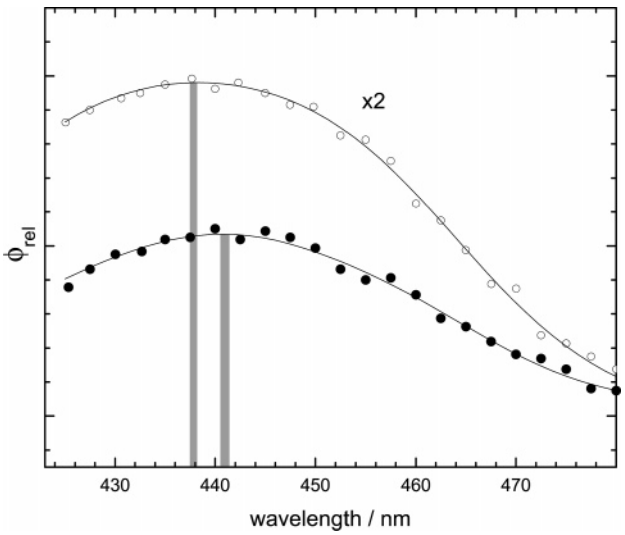

Figure 8. Photoionization spectra for NaCl/SDS (4.8%) at 20% RH in efflorescence mode (●) and deliquescence mode (○). The positions of the vertical lines mark the fitted value of λ_{max}, and the width represents the standard error in the fit.

surface is less polar than the KI surface,[23] producing a smaller red shift in the C314 spectroscopy.

IV. Discussion

Interpretation of ϕ_{rel}. Several factors related to the chemical environment of the C314 probe molecule influence the ionization efficiency in Figure 2. First, the surroundings serve as a perturbation on the electronic structure of the solute, making subtle changes in the molecular ionization cross section. Second, the size of the particle affects the ability of those photoelectrons that leave the surface to back diffuse to the particle and recombine. Last, the surroundings may also capture the nascent photoelectrons, preventing them from ever leaving the surface. Because we detect the net charge of the entire particle, any process that prevents photoelectrons from leaving the surface decreases the overall yield in our experiment.

Previous experiments[27] show that the change in ionization energy of C314 as a function of surface adsorbed water is relatively small compared to the total energy above threshold in these experiments, so we do not expect large changes in the ionization cross section. Because the number of probe molecules on each particle is determined by the dry size selection of the first DMA, the diameter changes associated with the hygroscopic growth of particles has little effect on ϕ_{rel} in the 100-nm size range. As a result, we expect that ϕ_{rel} mainly reflects changes in the ability of the surrounds to capture the photoelectron. Accordingly, of all the variables, ϕ_{rel} should be most sensitive to the amount and arrangement of water in the vicinity of the C314 probe molecule. We may also expect some dependence on the extent to which the probe molecule is buried by the surfactant molecules. The conclusions in this study depend very little on these considerations. All we require is that the probe molecule is sensitive to changes in its surroundings, and that sharp changes occurring over a small range of RH arise from phase changes. Nevertheless, interpreting the ϕ_{rel} data in this way does provide some additional insights.

Focusing on the water content alone is sufficient to explain the pure KI ϕ_{rel} data. The particles begin as aqueous droplets and shrink continuously as the RH decreases toward the ERH. The ϕ_{rel} curve is relatively flat in this region, because, although water is leaving the particle, it remains aqueous. The surroundings for the C314 molecule are relatively unchanged, aside from a steadily increasing concentration of dissolved ions. At the ERH, the slope of the ϕ_{rel} curve changes. Although the efflorescence represents a drastic morphological change, there is not a large step function change in ϕ_{rel} at the ERH as one might expect. From the point of view of the C314 probe molecule, though, there may still be a significant amount of water adsorbed to the surface. For example, for crystalline NaCl, there is on the order of one monolayer of adsorbed water on the surface near the ERH for a NaCl aerosol particle.[36] As the RH continues to drop, this surface adsorbed water desorbs, and the ϕ_{rel} increases accordingly.

Morphology of Surfactant-Coated Particles. A similar interpretation of the ϕ_{rel} to that for KI fits the mixed KI/SDS particles as well. The ϕ_{rel} is constant with falling RH until the ERH of the KI core, where it begins to increase. At this point, two limiting possibilities arise. When the SDS coverage is high ($>3.2\%$), the ϕ_{rel} curve adopts a positive curvature for RH < ERH, and an additional sharp feature is evident at low ($<5\%$) RH. The λ_{max} data (Figure 5) show that, in efflorescence mode, the C314 environment matches that of a water−organic interface rather than a solid KI surface until the RH drops below 5%. At this point, the spectroscopy transitions to the surface adsorbed value, and the ϕ_{rel} curve shows a corresponding sharp increase. Likewise, in the high coverage regime, the λ_{max} value at 20% RH shows the hysteresis behavior, confirming the existence of a phase transition between 0% and 5% RH.

We conclude that when there is sufficient SDS coverage, a thin soapy film remains on the surface following the efflorescence of the KI core. Figure 9 illustrates the proposed morphology of the particles before and after the core efflorescence. The thin SDS film supported on the crystalline substrate contains enough water to solvate the sulfate head groups and their counterions. This structure is reminiscent of a soap black film, which is a quasi-stable bilayer of surfactant separated by a layer of water and is associated with foams and bubbles. Newton black films (NBF's), which have water layers thinner than 1 nm,[37] are most similar to the structure we propose here. We do not suggest, though, that the surfactant layer is necessarily as highly ordered as an NBF, especially at coverages exceeding one monolayer. At RH < 5%, this soapy film can

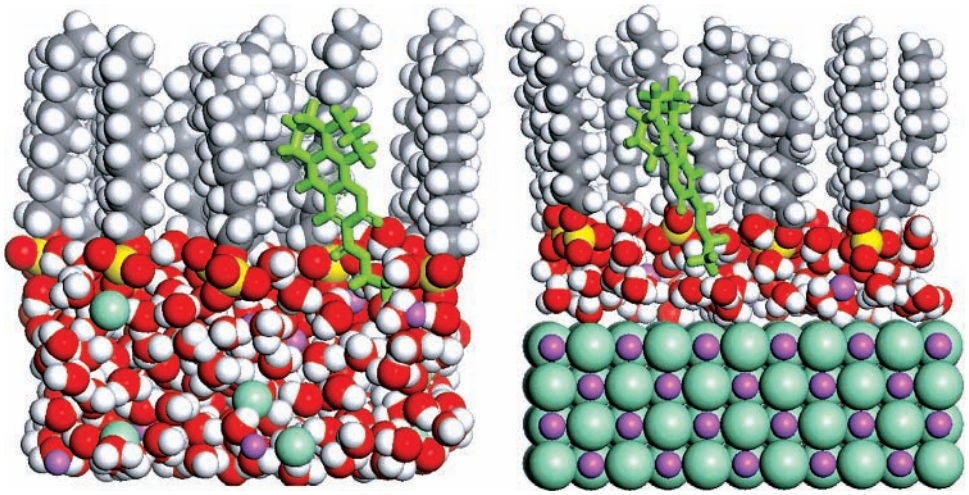

Figure 9. Particle surface before and after the efflorescence of the aqueous salt core. Prior to efflorescence (left side) the SDS molecules coat an aqueous solution of salt. Following efflorescence, when there is sufficient SDS, a thin soap film persists on the solid salt particle. The water, SDS, and salt ions are shown in a space-filling style, and the C314 probe molecule is shown in a tube style. The illustration is intended to convey the purposed structure on a coarse level; the orientation of the SDS molecules and the thickness of the water layer are not known.

undergo a separate efflorescence. The size change associated with this process is too small to be detected with our RH-TDMA apparatus.

We have no direct probe of the nature of the SDS below the thin film efflorescence point, but we can make some inferences by considering the C314 spectroscopy. The data suggest a picture where C314 is exposed to the KI surface rather than the organic fraction. One possibility is that the SDS forms three-dimensional crystallites on the surface, excluding the C314 and leaving it adsorbed to the KI surface. This picture explains both the change in the electronic spectroscopy as well as the sudden increase in the ϕ_{rel}. The C314 that was previously dissolved in the soap is now exposed, and the nascent photoelectron should escape the surface more efficiently.

A deliquescence mode experiment has this structure as its starting point, and increasing the RH results in the gradual adsorption of water to its surface. At RH below the DRH, the added water does not reform the thin soap film, as Figure 5 shows. The λ_{max} value remains high, indicative of the KI surface environment, until the RH approaches the DRH. The slight apparent decrease in the λ_{max} value over this RH range is consistent with previous measurements on pure NaCl particles[27] and may arise from the rearrangement of the KI lattice in the vicinity of the C314 molecules.

At low SDS coverages (i.e., SDS $<$ 1.6%), the ϕ_{rel} curves are similar to that of pure KI. In this regime, the λ_{max} value at 20% RH (446 nm) is indicative of the C314 adsorbed to the KI surface and not associated with a water−organic interface. Further, λ_{max} is independent of the data collection mode (i.e., no hysteresis effect), so there is no indication of a low-RH phase transition. One possibility is that no thin film remains on the particle following the efflorescence of the core KI. This scenario is consistent with both the similarity between the pure KI and KI/SDS ϕ_{rel} curves and the λ_{max} data that suggest that C314 is associated with the surface. A second possibility is that the film forms only in patches leaving the C314 adsorbed to the KI surface. The driving force for excluding the C314 from this film is not apparent, and we find that the former scenario is more likely. Likewise, a more quantitative examination of the surface SDS coverage also suggests that no film forms at low coverages.

Using the growth factors from Figure 1 and the experimentally set dry particle size of 100 nm, we can calculate the size of the aqueous particle at the DRH to be 135 nm. The surface area of this particle is 5.73×10^4 nm^2. Saturated SDS monolayers have an experimentally determined head group area of 0.33 nm^2 for NBF's[37] and between 0.4 nm^2 and 0.5 nm^2 for flat air−water interfaces.[38−40] For these calculations, we use an intermediate value of 0.40 nm^2, which closely matches the optimum value determined in a recent MD simulation.[41] Thus, for this size particle, such a footprint corresponds to 1.43×10^5 SDS molecules. At the DRH, the concentration of KI is approximately 8.4 M (the concentration of a saturated KI solution at 298 K). For the 4.8% SDS mixture, we can calculate the number of surfactant molecules associated with the particle to be 1.86×10^5. The SDS is not uniformly distributed in the particle, though. As we stated previously, we expect that the surfactant resides predominantly on the particle surface.

Defining the surface coverage, θ, as the ratio of SDS molecules on the surface to the maximum number in a stable monolayer, we find a value of $1.86 \times 10^5/1.43 \times 10^5 = 1.3$. This result indicates that at the DRH, the SDS film on this particle is approximately 1 monolayer. For the range of compositions in our experiment, the value of θ varies from 0.4 to 1.3 at the DRH. At the ERH, where the particles are 1.15 times smaller in diameter, these values range from 0.6 to 1.7. The smallest SDS composition in our experiment that clearly exhibits thin film formation is 3.2%. At the ERH, the value of θ for this mixture is approximately 1.1. We can conclude that the formation of the soapy layer depends on the proximity of SDS molecules. Submonolayer coverages have insufficient coupling between SDS molecules to retain a uniform layer, whereas dense films do.

The signal magnitudes for NaCl/SDS are smaller than for KI/SDS, and the contrast between the spectroscopy of NaCl surface and the water−surfactant interface is not as great. As a result, the data for NaCl/SDS do not provide as clear a picture as the KI/SDS case. The available data, though, lead to similar conclusions. The ϕ_{rel} curve for pure NaCl is much flatter below the ERH, implying that there is less water in the vicinity of the C314 in that case. The 4.8% SDS particles, though, show a sloped curve, just as for the KI/SDS case. Figure 9 demonstrates the hysteresis effect found for the SDS-rich particles. We conclude that the formation of a thin SDS film similarly accounts for these observations as well.

Consequences for Atmospheric Chemistry. Several important heterogeneous reactions in the troposphere depend strongly on the amount and accessibility liquid water associated with the particle. A prominent example is the heterogeneous hydrolysis of N_2O_5.[11,12,42,43] As we discussed in the Introduction, surfactant monolayers have been shown to decrease the uptake coefficient for this reaction by as much as an order of magnitude by limiting the mass transfer across the interface.[12] Our results suggest other potential consequences of these surfactant layers. At values of RH lower than the core ERH, the amount and character of liquid water depends upon the RH, the amount of surfactant, and conditionally on the history of the particle. At 20% RH, the water is buried by a dense organic coating when the thin film is present but exists mainly as surface adsorbed water if the thin film had previously effloresced in an arid environment. These results may also inform future laboratory studies that employ surfactant-coated particles, where differences in the preparation and handling of the particles may give rise to different morphologies.

Our intent is to model surfactant-coated particles of marine origin, but the differences between our model particles and real marine particles are significant. For example, sea spray comprises several different salts rather than just a single component. Also, the organic fraction is better represented by long-chain carboxylic acids than SDS, and the acids are primarily molecular rather than ionic. Nonetheless, there is ample reason to conclude that our results may be quite general from a qualitative standpoint. First, mixed salts tend to segregate into domains when exposed to water.[44,45] The thin film behavior may be confined to certain regions of the surface of a mixed particle, but still be present. Further, the degree of dissociation of SDS in NBF's is likely lower than that of a typical aqueous solution of SDS,[46] giving the head groups the dipolar character of a non-ionic surfactant. This situation arises from the low dielectric constant of the interfacial water.[47] The films formed in our experiment may show similar behavior, minimizing the distinction between ionic and non-ionic surfactants.

V. Conclusion

The surface morphology of SDS-coated salt particles depends strongly on the amount of surfactant and the RH. The possible configurations of the surface include that of an aqueous surfactant monolayer, a thin soap film supported on a salt core, and an internal mixture of solid salt and solid SDS. When the coverage of SDS is in the monolayer range, a thin soap film persists on the particle surface at a RH below the ERH of the core salt. This thin film can undergo a separate efflorescence, leading to a hysteresis in the particle morphology over a wide range of RH.

Acknowledgment. This work was supported by a Research Corporation Cottrell College Science Award and the American Chemical Society Petroleum Research Fund.

References and Notes

(1) Jacobson, M. C.; Hansson, H. C.; Noone, K. J.; Charlson, R. J. *Rev. Geophys.* **2000**, *38*, 267.

(2) McMurry, P. H. *Atmos. Environ.* **1999**, *34*, 1959.

(3) Tervahattu, H.; Hartonen, K.; Kerminen, V.; Kupiainen, K.; Aarnio, P.; Koskentalo, T.; Tuck, A.; Vaida, V. *J. Geophys. Res.—Atmos.* **2002**, *107*.

(4) Tervahattu, H.; Juhanoja, J.; Kupiainen, K. *J. Geophys. Res.—Atmos.* **2002**, *107*.

(5) Tervahattu, H.; Juhanoja, J.; Vaida, V.; Tuck, A.; Niemi, J.; Kupiainen, K.; Kulmala, M.; Vehkamaki, H. *J. Geophys. Res.—Atmos.* **2005**, *110*.

(6) Barney, W. S.; Morris, J. W.; Shi, Q.; Jayne, J. T.; Jimenez, J. L.; Kolb, C. E.; Davidovits, P.; Cass, G. R.; Worsnop, D. R. *Abstr. Pap. Am. Chem. Soc.* **2000**, *220*, U346.

(7) Moise, T.; Rudich, Y. *J. Phys. Chem. A* **2002**, *106*, 6469.

(8) Smith, G. D.; Woods, E.; DeForest, C. L.; Baer, T.; Miller, R. E. *J. Phys. Chem. A* **2002**, *106*, 8085.

(9) Thornberry, T.; Abbatt, J. P. D. *Phys. Chem. Chem. Phys.* **2004**, *6*, 84.

(10) Rogge, W. F.; Hildemann, L. M.; Mazurek, M. A.; Cass, G. R.; Simonelt, B. R. T. *Environ. Sci. Technol.* **1991**, *25*, 1112.

(11) Thornton, J.; Abbatt, J. *J. Phys. Chem. A* **2005**, *109*, 10004.

(12) McNeill, V. F.; Patterson, J.; Wolfe, G. M.; Thornton, J. A. *Atmos. Chem. Phys.* **2006**, *6*, 1635.

(13) Ellison, G. B.; Tuck, A. F.; Vaida, V. *J. Geophys. Res.—Atmos.* **1999**, *104*, 11633.

(14) Martin, S. T. *Chem. Rev.* **2000**, *100*, 3403.

(15) Brooks, S. D.; Garland, R. M.; Wise, M. E.; Prenni, A. J.; Cushing, M.; Hewitt, E.; Tolbert, M. A. *J. Geophys. Res.—Atmos.* **2003**, *108*, ACH23/1.

(16) Braban, C. F.; Carroll, M. F.; Styler, S. A.; Abbatt, J. P. D. *J. Phys. Chem. A* **2003**, *107*, 6594.

(17) Badger, C. L.; George, I.; Griffiths, P. T.; Braban, C. F.; Cox, R. A.; Abbatt, J. P. D. *Atmos. Chem. Phys.* **2006**, *6*, 755.

(18) Parsons, M. T.; Knopf, D. A.; Bertram, A. K. *J. Phys. Chem. A* **2004**, *108*, 11600.

(19) Takahama, S.; Pathak, P. K.; Pandis, S. N. *Environ. Sci. Technol.* **2007**, *41*, 2289.

(20) Chen, Y. Y.; Lee, W. M. G. *J. Environ. Sci. Health* **2001**, *A32*, 229.

(21) Choi, M. Y.; Chan, C. K. *J. Phys. Chem. A* **2005**, *109*, 1042.

(22) Choi, M. Y.; Chan, C. K.; Zhang, Y. H. *J. Phys. Chem. A* **2004**, *108*, 1133.

(23) Woods, E., III; Wivagg, C. N.; Chung, D. *J. Phys. Chem. A* **2007**, *111*, 3336.

(24) Matter, D.; Mohr, M.; Fendel, W.; Schmidt-Ott, A.; Burtscher, H. *J. Aerosol Sci.* **1995**, *26*, 1101.

(25) Niessner, R. *J. Aerosol Sci.* **1986**, *17*, 705.

(26) Niessner, R.; Wilcox, C. F. *Anal. Chem.* **1989**, *61*, 708.

(27) Woods, E.; Morris, S. F.; Wivagg, C. N.; Healy, L. E. *J. Phys. Chem. A* **2005**, *109*, 10702.

(28) Rader, D. J.; McMurry, P. H. *J. Aerosol Sci.* **1986**, *17*, 771.

(29) Li, W.; Montassier, N.; Hopke, P. K. *Aerosol Sci. Technol.* **1992**, *17*, 25.

(30) Cziczo, D. J.; Nowak, J. B.; Hu, J. H.; Abbatt, J. P. D. *J. Geophys. Res.—Atmos.* **1997**, *102*, 18843.

(31) Richardson, C. B.; Snyder, T. D. *Langmuir* **1994**, *10*, 2462.

(32) Cohen, M. D.; Flagan, R. C.; Seinfeld, J. H. *J. Phys. Chem.* **1987**, *91*, 4563.

(33) Cohen, M. D.; Flagan, R. C.; Seinfeld, J. H. *J. Phys. Chem.* **1987**, *91*, 4583.

(34) Wang, H.; Borguet, E.; Eisenthal, K. B. *J. Phys. Chem. B* **1998**, *102*, 4927.

(35) Steel, W. H.; Walker, R. A. *Nature* **2003**, *424*, 296.

(36) Foster, M. C.; Ewing, G. E. *J. Chem. Phys.* **2000**, *112*, 6817.

(37) Belorgey, O.; Benattar, J. *Phys. Rev. Lett.* **1991**, *66*, 313.

(38) Kawai, T.; Kamio, H.; Kondo, T.; Kon-No, K. *J. Phys. Chem. B* **2005**, *109*, 4497.

(39) Matijavic, E.; Pethica, B. A. *Trans. Faraday Soc.* **1958**, *54*, 1383.

(40) Persson, C. M.; Jonsson, A. P.; Bergstrom, M.; Eriksson, J. C. *J. Colloid Interface Sci.* **2003**, *267*, 151.

(41) Jang, S. S.; Goddard, W. A. *J. Phys. Chem. B* **2006**, *110*, 7992.

(42) Leu, M. T.; Timonen, R. S.; Keyser, L. F.; Yung, Y. L. *J. Phys. Chem.* **1995**, *99*, 13203.

(43) Thornton, J.; Braban, C.; Abbatt, J. *Phys. Chem. Chem. Phys.* **2003**, *5*, 4593.

(44) Allen, H. C.; Laux, J. M.; Vogt, R.; Finlayson-Pitts, B. J.; Hemminger, J. C. *J. Phys. Chem.* **1996**, *100*, 6371.

(45) Ghosal, S.; Shbeeb, A.; Hemminger, J. C. *Geophys. Res. Lett.* **2000**, *27*, 1879.

(46) Ruckenstein, E.; Manciu, M. *Langmuir* **2002**, *18*, 2727.

(47) Faraudo, J.; Bresme, F. *Phys. Rev. Lett.* **2004**, *92*.